**PAPER • OPEN ACCESS**

# Parametric Design Tool for Development of a Radial Guide Vane Cascade for a Variable Speed Francis Turbine

View the article online for updates and enhancements.

# Parametric Design Tool for Development of a Radial Guide Vane Cascade for a Variable Speed Francis Turbine

**Filip Stojkovski, Marija Lazarevikj, Zoran Markov**

Ss."Cyril and Methodius" University in Skopje, Faculty of Mechanical Engineering
Skopje, Rugjer Boshkovikj 18, 1000 Skopje, Republic of North Macedonia

Corresponding author: filip_stojkovski@outlook.com

**Abstract**. Hydropower as a part of the family of renewable energy sources represents an engineering and scientific field which inspires researchers to work on development of the systems and sub-systems in a way of optimizing the whole energy transformation process to obtain more efficient, flexible and reliable hydropower operation with the best possible water to energy ratio. This research is part of a Horizon 2020 HydroFlex project by the Norwegian University of Science and Technology (NTNU), where the main goal is development of a flexible hydropower generation. The guide vane cascade is one of the most crucial stationary sub-systems of the hydraulic turbine and is a subject of this study. Its re-design for obtaining a quality "flow-feeding" of a variable speed high head Francis turbine is developed. Having this goal in mind, a MATLAB code was generated, based on several key parameters, such as initial energy conditions as net head and turbine discharge at best efficiency point (BEP). Turbine runner geometrical constraints are taken into account during this process, while using recommendations for some initial guide vane calculations such as their number, inlet and outlet diameter, guide vane axis diameter, delivery angles etc. Using an inverse Euler turbine equation, the operating range of the turbine was calculated for a variable speed and discharge conditions, keeping the shock-free flow for all states at the runner's inlet, as it is the most favourable inflow condition. For those operating points, the flow streamlines angles were obtained at the guide vanes leading and trailing edges. With an interpolating mathematical functions between the angles of the leading and trailing edges, the camber lines of the hydrofoils were obtained for further guide vane cascade geometry development. This algorithm can be implemented on any given runner geometry. The guide vane design is then exported into ANSYS Workbench for further numerical tests, such as CFD simulations for verifying the hydrodynamic characteristics and FEM analysis for verifying the structural integrity of this sub-system for variable speed operating conditions.

**Keywords:** Guide Vanes, Parametric Design, Variable Speed, Francis Turbines

## 1. Introduction

Increasing flexibility in energy production from hydropower plants is a task demanded by the hydropower sector in Europe and worldwide, especially at off-design operation conditions of the turbines. Using flexibility, variable speed operation (VSO) can be implemented to perform more efficient energy production at off-design operating conditions. As part of the HydroFlex project, the goal of this research is to develop a parameter based code for generating favourable designs of a radial guide vane cascade for low specific speed Francis turbines. In this case, the code was developed for the existing Francis 99 turbine runner from the open source web-site of the Waterpower Laboratory [11] at NTNU, but the research shows that it can be generalized for various high head Francis turbine runners.

To start with, the theoretical background was implemented and researched by using the classic turbine theory to obtain the one-dimensional mathematical relations which describe the flow conditions in the guide vanes, especially the flow conditions between the guide vanes and the runner. Secondly, the physics of variable speed turbine was studied and mathematically simplified as one dimensional models to obtain the relations and dominant parameters which need to be examined. Next, a matrix based calculation was performed to obtain the operating ranges of the turbine and the guide vanes openings

for settled range of rotational speed and discharges, by keeping constant head as the situation is observed as steady state.

The geometry of the radial cascade blades was developed by using recommendations for developing a 4 digit NACA hydrofoils and by implementing the camber and thickness functions. As previously the operating ranges of the turbine were calculated, following the one dimensional mid-span streamline curvature at the inlet and outlet of the guide vanes, by interpolating the hydrofoil camber functions, the camber line of the blade was obtained, and the thickness was obtained from other static calculations. Later, the initially obtained geometry was tested with Computational Fluid Dynamics (CFD) simulations for the previously given operating conditions and it was compared with the numerically obtained results for the existing guide vanes of the Francis 99 turbine.

## 2. Theoretical Background

During turbine operation, flow to the runner is managed by the guide vanes and depending on the opening position, turbine torque varies. The guide vane is the stationary component, and the runner is the rotating component of a turbine. We can represent the flow conditions between the guide vanes and the runner inlet i.e. in the vaneless space, considering the equation of motion of an ideal fluid in the vector form Lamb – Gromeko [2,3]:

$$\frac{\partial \vec{V}}{\partial t} + \vec{\Omega} \times \vec{V} = -grad(gH) \tag{1}$$

where $H$ is the specific energy of the fluid in absolute movement, $\vec{V} = \left(\vec{V_z}, \vec{V_r}, \vec{V_u}\right)$ is the absolute velocity vector having components in a cylindrical coordinate system, and $\vec{\Omega} = rot\vec{V}$ is the vortex vector whose projections on the axis of the cylindrical coordinate system are equal to:
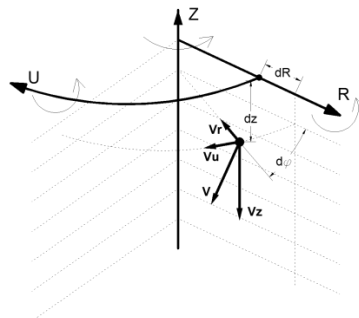


$$\Omega_r = \frac{\partial v_z}{\partial \varphi} - \frac{\partial v_u}{\partial z}$$

$$\Omega_z = -\frac{\partial v_u}{\partial r} + \frac{\partial v_r}{\partial \varphi} \tag{2}$$

$$\Omega_u = -\frac{\partial v_r}{\partial z} + \frac{\partial v_z}{\partial r}$$

Fig.1. Absolute flow vector and its components in cylindrical coordinate system for the vaneless space

Experimental studies show that in the area between the guide vanes and the runner, the fluid motion with sufficient accuracy can be considered steady and axisymmetric. With reasonable accuracy, we can also accept that in front of runner, the specific energy of the fluid is constant. In that case, for steady flow and for axisymmetric conditions:

$$\frac{\partial \vec{V}}{\partial t} = 0 \; ; \; \frac{\partial(v, H)}{\partial \varphi} = 0 \tag{3}$$

Two flow modules can be observed, i.e. the flow is **potential**, or the flow is **rotational (helical type)**. For potential flow it can be derived that there are no changes in the velocity in the radial direction:

$$\frac{\partial(v_u r)}{\partial z} dz + \frac{\partial(v_u r)}{\partial r} dr + \frac{\partial v_u}{r \partial \varphi} r d\varphi = d(v_u r) = 0 \tag{4}$$

and for helical flow, the vortex vector and the velocity vector are parallel to each other, i.e.:

$$d(v_u r) = \frac{\partial v_u}{\partial r} dr + \frac{\partial v_u}{\partial z} dz = 0 \tag{5}$$

From both cases the "free vortex" equation can be derived, which shows that the circulation created by the guide vanes in the vanelesss space preserves:

$$\Gamma = \oint v_u \, dl = 2r\pi \cdot v_u = const. \tag{6}$$

According to this, several conclusions can be derived:

- The guide vanes form a steady axisymmetric flow in front of the runner, which is either potential or rotational
- In the case of potential flow, the swirl is constant for all points of the liquid in the region between the guide vanes and the runner
- In the case of a rotational flow, the swirl of the flow maintains a constant value along the streamline and changes from one streamline to another

Let's consider in what cases behind the guide vanes potential or helical flow is formed. This is mainly determined by the outlines of the flowing part in the area between the guide apparatus and the runner, and also depends on the height of the guide apparatus. In the present case, a high-head Francis turbine runner is studied. The leading edge of the runner blade is located in the zone of radial movement of the liquid and represents a vertical line, i.e., $r_1 \approx const.$ along the leading edge of the runner blade.
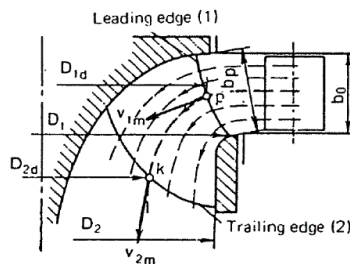


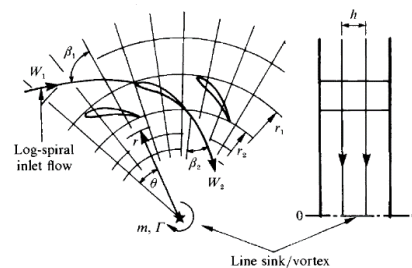Fig.2. Flow path of Radial-axial hydraulic turbine [1]      Fig.3. Radial cascades [5]

Following the classic turbine theory, a mean mid-span streamline method was used to develop the mathematical relations valid for the guide vanes outlet i.e. runner inlet conditions. The water flow in front of the runner is formed by the annular (radial) cascade of guide vanes, which is characterized by the form of the blade profiles and the chord spacing of the cascade [1]. The blade profile can be symmetric if the camber line of the profile is represented by straight line, or asymmetric if the camber line of the profile is curved. The cascade is defined by the pitch, which means the distance between two blades in the row, and the chord length of the blades. The ratio of the chord length and the pitch, i.e. $L/t$ indicates the cascade density. As the guide vane must ensure complete closure of the turbine runner, the ratio $L/t$ is greater than unity, which shows that the cascade is sufficiently dense, and by that, it can be assumed that the direction of water velocity is very close to the direction of the blades outlet edges. For radial-flow cascade, the vector of absolute water flow can be presented as a sum of two vector components: the radial (meridian) component and the peripheral (circulation) component:

$$\overrightarrow{v_0} = \overrightarrow{v_{0r}} + \overrightarrow{v_{0u}} \tag{7}$$

Knowing the flow rate through the turbine and the dimensions (height) of the guide vanes, the radial component can be specified as:

$$v_{0r} = \frac{Q}{D_{o2}\pi B_o} \tag{8}$$

The angle between the vector components is derived from the geometry relation of the guide vanes opening as:
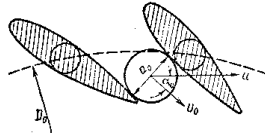


$$v_0 = \frac{v_{0r}}{sin\alpha_0} \; ; v_{0u} = v_0 cos\alpha_0 \qquad (9)$$

Fig.4. Guide vanes opening parameters [4]

The flow conditions just in front of the runner, for high-head (low-speed) turbines, in a relation with the constant circulation created from the guide vanes (eq.6), the velocity parallelograms can be related as:



Fig.5. Velocity parallelograms [1]
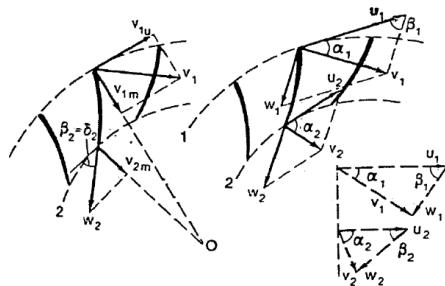
$$v_{1m} = \frac{Q}{D_{1d}\pi B_1}$$

$$v_{1u} = v_{0u} \cdot \frac{D_{o2}}{D_{1d}}$$

$$v_1 = v_{1m} + v_{1u} \qquad (10)$$

$$u_1 = \frac{D_{1d} \cdot \pi \cdot n}{60}$$

Including the Euler turbine equation, the torque and the energy created in the runner can be written as:

$$\sum M_0 = \rho Q(r_1 c_{1u} - r_2 c_{2u}) = \frac{\rho Q}{2\pi}(\Gamma_1 - \Gamma_2) \qquad (11)$$

$$gH\eta_h = u_1 c_{1u} - u_2 c_{2u} = \frac{\omega}{2\pi}(\Gamma_1 - \Gamma_2) \qquad (12)$$

from which several essential conclusions can be considered:

- The principal importance is the structure of the flow in front and behind the runner.
- Most favourable operating condition regarding the efficiency is the outlet circulation $\Gamma_2 \approx 0$; where the front circulation is constant and can be estimated as $\Gamma_1 \approx \Gamma_0 \approx const.$ from the circulation created behind the guide vanes.
- Most favourable inflow conditions can be estimated when shock-free (zero-incidence) entry in the runner is provided, i.e. the leading edge angle remains constant $\beta_1 = const.$

Previous explanations are derived for constant rotational velocity of the runner. The variable speed operation assumptions regarding the guide vanes, can be derived from the Euler equation observing the possibility of flow regulation with the guide vanes. After several mathematical operations, the flow regulation can be expressed as [3]:

$$Q = \frac{\left(\frac{gH\eta_h}{\omega}\right) + (\omega r_2^2)}{\left(\frac{ctg\alpha_0}{2\pi B_{o1}}\right) + \left(\frac{r_2 ctg\beta_2}{A_2}\right)} \;\; \rightarrow \;\; ctg\alpha_0 = \left[\frac{\left(\frac{gH\eta_h}{\omega}\right) + (\omega r_2^2)}{Q} - \left(\frac{r_2 ctg\beta_2}{A_2}\right)\right] \cdot 2\pi B_{o1} \qquad (13)$$

where $Q$ is the flow rate, $\omega$ is the angular velocity of the runner, $\alpha_0$ is the guide vanes outlet angle (fig.4), $\beta_2$ is the runner blades trailing edge angle (fig.5) and $A_2$ is the runner outlet surface. In the case that it is analysed, this equation was implemented in the previously tested operating region of the turbine, which is described later in this paper. The physical phenomenon of variable speed used at high-head (low-speed) turbines, keeping the head constant, at constant guide vanes opening, can be written as:

30th IAHR Symposium on Hydraulic Machinery and Systems

IOP Conf. Series: Earth and Environmental Science **774** (2021) 012112

IOP Publishing

doi:10.1088/1755-1315/774/1/012112

$$u_2 < \sqrt{gH\eta_h} \tag{14}$$

which shows that the flow rate decreases with the increasing of the rotational speed of the runner [4]. Physically this can be described as the near positioning of the runner blades and the guide vanes, when the rotational speed increases, the rotational "frames" created of the runner blades inner channels are more frequent and they are "repelling" the amount of flow, in other case when the rotational speed decreases, the rotational "frames" of the runner blades inner channels are less frequent and the runner is absorbing increased amount of flow, observing runner with fixed number of blades. This shows how the runners rotational speed influence on the flow rate, for constant head and constant guide vanes opening [4]:

$$A \cdot \frac{dQ}{d\omega} = \frac{u_2^2 - gH\eta_h}{\omega^2} + \frac{gH}{\omega} \cdot \frac{d\eta_h}{d\omega} \tag{15}$$

where A is positive number, and the change of the hydraulic efficiency with the rotational velocity can be neglected for further simplifications.

## 3. Hydrodynamic profile of a guide vane

Profiling the hydrofoil of the guide vanes by using the derived one-dimensional relations can be made with several easy steps. Observing the hydrofoil camber line, for the calculated velocities and streamlines angles for the BEP of the turbine, we can "interpolate" the camber line as a function between the streamlines angles, taking into account the previously assumptions for most favourable inflow conditions. Observing fig.3. we can conclude that the guide vane hydrofoil camber is positioned in a way that the leading edge of the hydrofoil is corresponding with the spiral case and stay vanes outlet angle of the absolute velocity vector. The trailing edge of the guide vane hydrofoil shall be in accordance with the guide vanes outlet angle (fig.4) i.e. $\alpha_0 \approx \alpha_1$, previously calculated for various runner inflow conditions. The NACA standards, are recommending equations for describing the geometry of their 4-digit MPXX hydrofoils, such as [10]:

$$y_{c1} = \frac{M}{P^2}(2Px - x^2)\,;for\ 0 < x < P \tag{16}$$

$$y_{c2} = \frac{M}{(1-P)^2}[(1-2P) + 2Px - x^2]\,;for\ P < x < c \tag{17}$$

where eq.16 describes the law of camber-line distribution from the beginning to the location of maximal camber deflection and eq.17 describes the camber-line distribution from the maximal camber location to the full length of the chord line 'c', M defines the maximal camber deflection and P is the location of maximal camber. The thickness distribution above and below of the hydrofoil is described as:

$$\pm y_t = \frac{t}{0{,}2}\left(a_0\sqrt{x} - a_1 x - a_2 x^2 + a_3 x^3 - a_4 x^4\right) \tag{18}$$

$$a_0 = 0{,}2969\,[-]; a_1 = 0{,}1260\,[-]; a_2 = 0{,}3516\,[-]; a_3 = 0{,}2843\,[-]; a_4 = 0{,}1015\,[-] \tag{19}$$

The coordinate points for the hydrofoil up/low contour lines are calculated as:

$$tan(\theta) = \frac{dy_{ci}}{dx} \tag{20}$$

$$x_U = x - y_t \cdot sin\theta\,;\ y_U = y_{ci} + y_t \cdot cos\theta \tag{21}$$

$$x_L = x + y_t \cdot sin\theta\,;\ y_L = y_{ci} - y_t \cdot cos\theta \tag{22}$$

where $x_U, y_U, x_L$ and $y_L$ are the coordinates of the upper/lower curves respectively, and $\theta$ is the angle of the camber increment. The equations for the camber line can be equalized for M and P as the camber is represented by two functions having the same camber criterions - parameters. Using the tangency rule for the leading and trailing edge angles of the foil, with the eq.20, we can simply represent that the first camber function is strictly dependent from the leading edge angle, and the second camber function from

the trailing edge angle. Developing a system of two equations and representing M and P as two variables, for previously calculated angles of the leading edge (the angle of the stay vanes outflow) and trailing edge (delivery angle of the guide vanes), we can determine the M and P parameter of the hydrofoil for the calculated streamline angles:

$$P^2 \cdot [tg\alpha_0 - tg\alpha_{svo}] - P \cdot [2tg\alpha_0 + tg\alpha_{svo}] + tg\alpha_0 = 0 \tag{23}$$
$$P \cdot tg\alpha_{svo} - 2 \cdot M = 0 \tag{24}$$

Solving this system of equations gives the values of M and P, and then by implementing those values, by using the equations of the camber line, the hydrofoil geometry is determined.

## 4. Parametric Design Tool - Initial Calculations and Geometry Development

All of the above equations and calculation procedure is implemented into a MATLAB code which is performing calculations for deriving the initial geometry of the radial guide vane cascade, where all previously described assumptions and simplifications are respected. First, the theoretical velocity triangles for the given runner geometry are calculated for obtaining the location of the best efficiency point. After that, the code is developed for calculating the velocity parallelograms for the vaneless space between the guide vanes and the runner, and also at the guide vanes inlet (constraints from the spiral case and stay vanes distributors). The number, diameters and pivot diameter for the guide vanes are calculated acc. to recommendations from the literature, which gives us space for further optimization including these variables. As it was mentioned, the principle of variable speed was implemented. For the given runner and measured model data, a flow and speed range were determined in the working area of the runner. According to eq.13, as the runner speed and flow are changing, disregarding the changes in the head (eq.3), the resulting variable is the guide vane flow delivery angle. All results are represented in relative values.

| Q [m3/s] | 0,21 |
|---|---|
| H [m] | 12,38 |
| n [rpm] | 333,33 |
| ned [-] | 0,176 |
| Qed [-] | 0,156 |
| Dgv1 [m] | 0,8 |
| Dgv2 [m] | 0,65 |
| Dgv_ax [-] | 0,71 |
| Bgv [m] | 0,06 |
| ngv [-] | 28 |
| alfa_gvo [deg] | 10,103 |

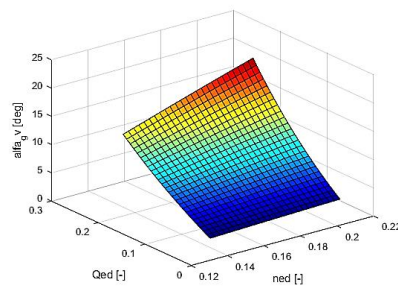Tab.1. Turbine and Guide Vanes Calculated Design Parameters



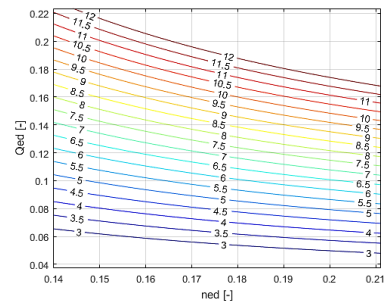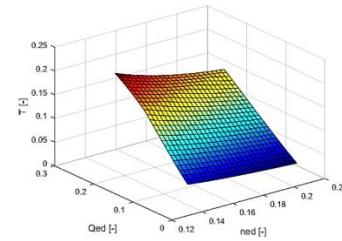Fig.6. Guide vanes delivery angles H=const.;Q=var.; n=var



Fig.7. Guide vanes delivery angles H=const.;Q=var.; n=var

From the charts on fig.6 and 7, it can be concluded that the guide vanes flow delivery angle increases with the rate of increased flow and runner speed. The function curvature is concave instead of convex because the losses through the guide vanes are neglected. The range on the 3D surface plot shows the maximal opening the guide vanes can have in the defined range of calculation for the machine, and the range on the 2D contour plot is constrained within the range up to 12 [deg] where later CFD calculations are performed. Using simplified mathematical models for the hydraulic losses in the turbine and with the indirect method for determining the efficiency, the theoretical hill chart was calculated using the one-dimensional theory developed before for the mid-streamline, within the runners operating domain, and also the mechanical torque that the runner can produce for these conditions.
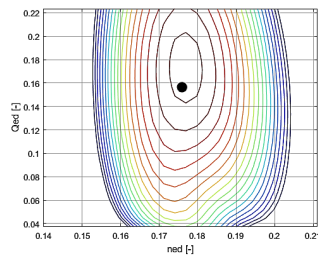
Fig.8. Predicted turbine hill (H=const.;Q=var.; n=var)          Fig.9. Runner Torque (H=const.;Q=var.; n=var)

From the predicted hill chart it can be concluded that the previously calculated BEP corresponds with the iso-lines for the zone of maximal predicted efficiency. From the chart on fig.9, it is evident that the torque increases with the increased amounts of discharge and reduced runner's speed. The point of variable speed in our case is to catch and connect the local best efficiency points of the turbine in different operating conditions. As expected, for keeping the head constant, and changing the guide vanes opening and runner rotational speed, we will obtain a similar behavior as double regulated turbine. Using the relations described in part 3, a guide vane hydrofoil is developed for the BEP and a radial guide vane cascade is plotted, which is later exported into ANSYS Workbench and ANSYS CFX for further CFD analysis.
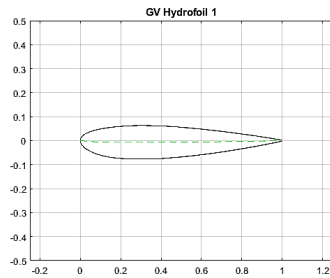


Fig.10. Developed guide vane hydrofoil
(M = -0,7265 ; P = 1,7738 ; XX=14%)          Fig.11. Guide vanes radial cascade plot
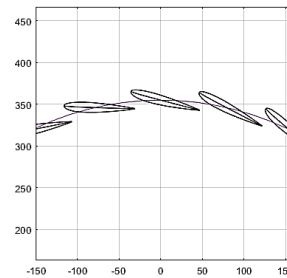
## 5. CFD Analysis

Two CFD models were built, tested and compared for similar mesh sizes and identical conditions, i.e. tested for constant head and $\pm5\%$ off-design rotational speed. The first CFD model i.e. Model 0 is the original Francis 99 Turbine, where the guide vane cascade and runner performance ware examined and tested. Model 1 is represented with fig.10. from above, developed with the design tool. Comparison of the guide vanes hydrofoils is given on the figures 12 and 13.
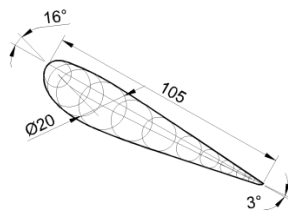


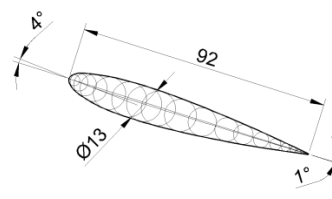Fig.12. Francis 99 – Hydrofoil (Model 0)          Fig.13. Developed Hydrofoil (Model 1)

According to the calculations in the design tool, the developed geometry of the blades in Model 1 is shorter. Also the thickness of the blade was calculated according to the maximal hydrostatic pressure for prototype pressure conditions, i.e. calculated as 14% of the blade chord length. The leading and trailing edge angles differs also as the NACA recommendations were implemented for 4 digit hydrofoils where the maximal camber and its location is strictly influenced from the calculated streamline angles, where in this case, it pulls behind the camber extension. The hydrofoil of Model 0 has a maximal thickness of 20% located at 20% chord length, compared to Model 1 where the maximal thickness is

30th IAHR Symposium on Hydraulic Machinery and Systems

IOP Conf. Series: Earth and Environmental Science **774** (2021) 012112

IOP Publishing

doi:10.1088/1755-1315/774/1/012112

14% located at 30% of the chord length. The pivot point of the blades in Model 1 is adopted to be at the gravity center of the blade. These calculations do not take into account the pivot point location, as the blade torque need to be examined via CFD simulation in some positions of partial opening to obtain a "zero torque". The numerical models are consisted of 3.3 - $3.4 \cdot 10^6$ cells. The number and size of the cells was selected according to previous performed CFD simulations of 3 operating points of the existing Francis 99 turbine model which showed good corresponding with the same points from the turbine hill chart. Zone mesh independence test for the guide vane domain was carried out, observing the total pressure drop through the cascade, for obtaining low deviations of the total pressure in front of the runner, i.e. the guide vanes outlet, where the number of cells from 0,4 to 1 million gave total pressure deviation of ±2%, so the meshes for the guide vanes were created within the range of $450-600 \cdot 10^3$ cells (fig.13.1.). The runner was consisted of $1.97 \cdot 10^6$ cells, the draft tube from $70 \cdot 10^3$ cells and the spiral casing with the stay vanes from $776 \cdot 10^3$ cells. The non-conformal meshes are connected with general grid interface. The boundary conditions of the models are set as constant inlet total pressure and outlet static pressure, i.e. the head is constant $H_n = 12,4 \ [m]$ as it was calculated within the design tool. Multiple openings for the guide vanes were taken into account to obtain the operating range of turbine. The simulations were guided as steady using the "Frozen Rotor" interface model for the runner. The selected turbulence model is standard $k - \varepsilon$ as it was previously tested for giving best predictions for the hydraulic character of the guide vanes blades [7] and the efficiency of the turbine [8]. The number of iterations was set to 1000, and the convergence of the results was successful reaching a residuals for the continuity up to RMS to $10^{-8}$ (fig.13.2).
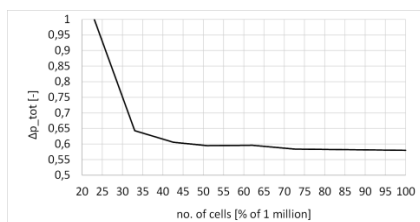


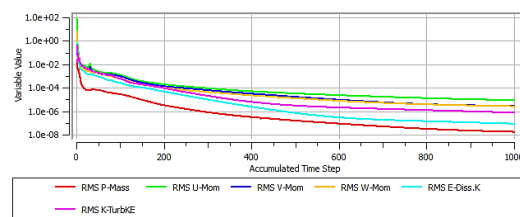Fig.13.1. Mesh independence test for the guide vanes



Fig.13.2. Convergence of residuals

The results obtained from the CFD simulations represented on a relative and non-dimensional scales for the discharge and the efficiency, where the calculated parameters for the Model 0 are the basis and the results from Model 1 are compared with them. The results for the head from the CFD calculations which are calculated according to IEC 60193 [13] varied cca. ±0,06% which is negligible. The efficiency is calculated as the ratio of mechanical power of the runner with the hydraulic power of the turbine, i.e.

$$\eta_t = \frac{P_m}{P_h} = \frac{T \cdot \omega}{\rho g H_n Q} \ [-] \tag{25}$$
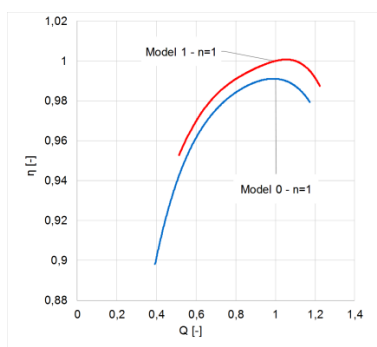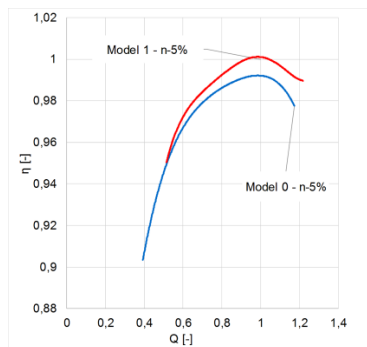


Fig.14. Turbine efficiency (n=1)
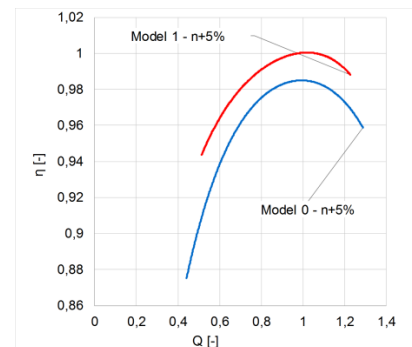


Fig.15. Turbine efficiency (n-5%)



Fig.16. Turbine efficiency (n+5%)

According to the charts it can be concluded that the efficiency is increased with using the guide vanes in Model 1. For runner design rotational speed (n=333,33 [rpm], i.e. n=1 [-]) the BEP location is shifted

to increased discharge from the location of the design basis BEP and the trend of the curve is similar with the basis curve. For runner rotational speed decreased by -5%, the local BEP location corresponds with the basis local BEP location, where it can be seen that the trend of the efficiency curve is not similar with the trend of the basis curve. For runner rotational speed increased by +5%, the local BEP location corresponds with the basis local BEP location and the trend of the curve is wider than the basis curve. By capturing the local best efficiency points and connecting them, a non-dimensional graph ($Q_{ed}$ [−], $n_{ed}$ [−]) was plotted for showing the trend of the connected BEPs.
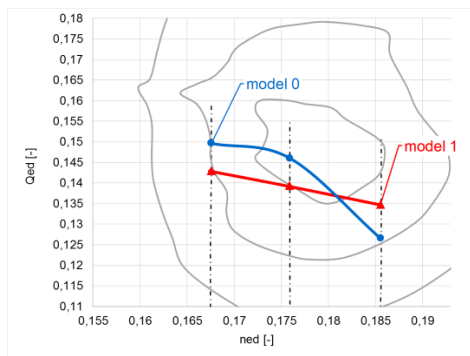


Fig.17. Connected local best efficiency points (hill efficiency zones are symbolic and generalized)
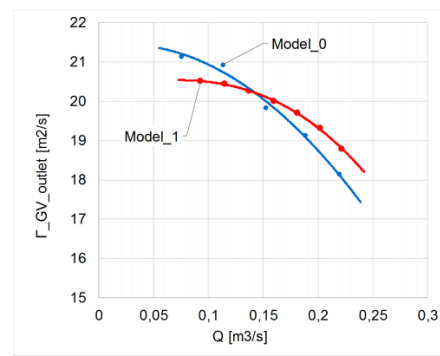


Fig.18. Guide Vanes outlet circulation v.s. flow rate

From the chart on fig.17. it can be concluded that the curve of the connected local BEP's for Model 1 is consistent showing how the runner's flow rate decreases with the increased rotational speed and vice versa. For Model 0 at n+5% it can be seen that the guide vanes are shifting the local BEP for a decreased flow rate. The guide vanes of Model 1 maintain higher outlet circulation which is one of the primary criteria for the efficiency of the guide vanes and the efficient "flow feeding" of high head turbines.
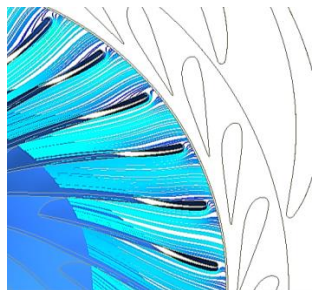


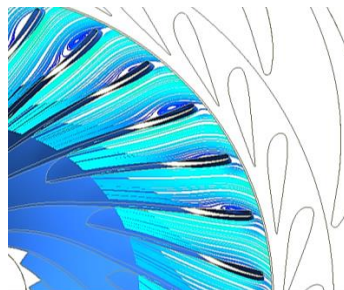Fig.19. Mid-span streamlines in runner (Model 0, n=1, Local BEP)



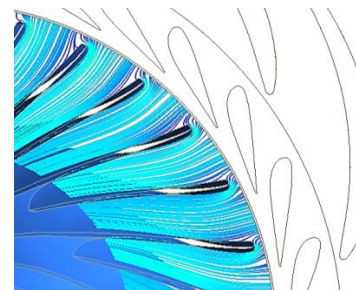Fig.20.Mid-span streamlines in runner (Model 0, n=+5%, Local BEP)



Fig.21. Mid-span streamlines in runner (Model 0, n=-5%, Local BEP)
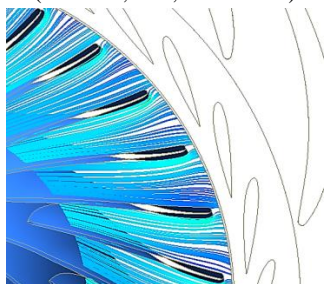


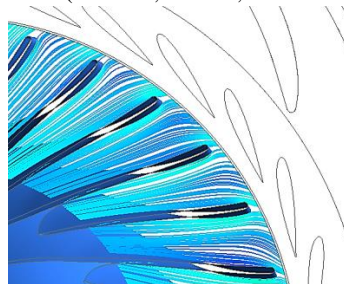Fig.22. Mid-span streamlines in runner (Model 1, n=1, Local BEP)



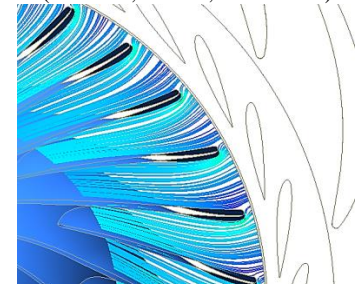Fig.23.Mid-span streamlines in runner (Model 1, n=+5%, Local BEP)



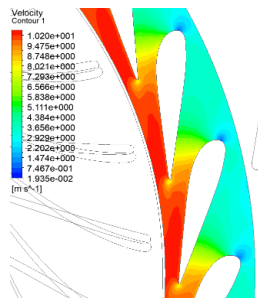Fig.24. Mid-span streamlines in runner (Model 1, n=-5%, Local BEP)
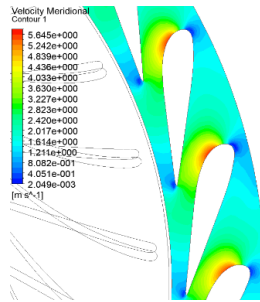
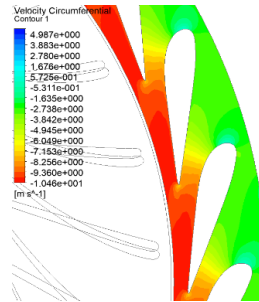Fig.25. Model 0 – Velocity


Fig.26. Model 0 – Meridian velocity


Fig.27. Model 0 – Circumferential Velocity

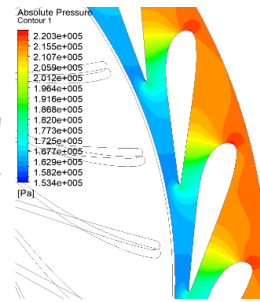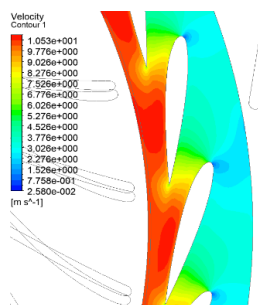
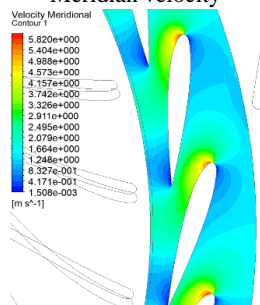Fig.28. Model 0 – Local Static pressure


Fig.29. Model 1 –Velocity
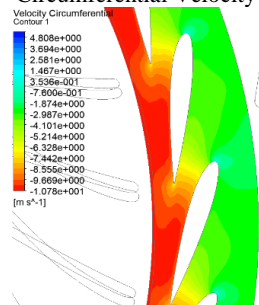

Fig.30. Model 1 – Meridian velocity


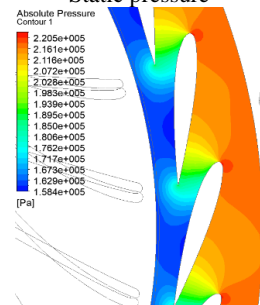Fig.31. Model 1 – Circumferential Velocity


Fig.32. Model 1 – Local Static pressure

The differences between the local BEP's is represented by the velocity profiles developed behind the guide vanes for both models, where a sc. "index of asymmetry" of the velocity profile is pointed out. It shows the ratio of the standard deviation of the mean velocities calculated along each point with the mean axial fluid velocity of the channel (in our case the meridian velocity on the pitch between 2 guide vane blades) [6]. The surface between the 2 blades is represented as a rectangular cross section with the blades pitch length and the blade height.

$$Y = \frac{\sigma_{Ui}}{U} = \frac{1}{U}\sqrt{\left[\frac{\sum_{i=1}^{n}(U_i - U)^2}{n - 1}\right]} \tag{26}$$
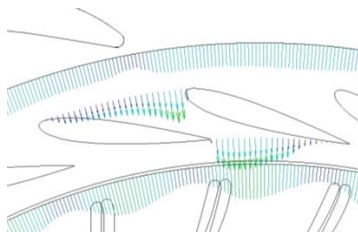

Fig.33. Meridian velocity profiles
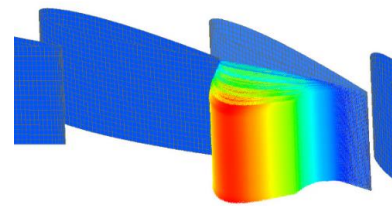

Fig.34. 3D Meridian velocity profile

On fig.33 it can be seen that the meridian (radial) velocities are not constant despite the assumption of simplification presented in eq.3. The guide vanes are creating crests which disrupt the velocity vector field in the vaneless space. Also because the angular change at constant radius, a localization of the maximal meridian vector was obtained near the first (left) blade. The velocity profile is disturbed along the guide vanes height because the skin friction between the top and low guide vanes rings. All of all, a 3D deformed meridian velocity vector profile is obtained which needs to be examined. If we neglect the deformity of the velocity profile along the guide vanes height, we can extract the angular change of the meridian velocity which is dominant in cases like this.

Fig.35. Comparison of the meridian velocity profiles for Model 0 and Model 1 at n=1 [-]; BEP



Fig.36. Relative deviation of the partial velocity vectors from the average velocity vector
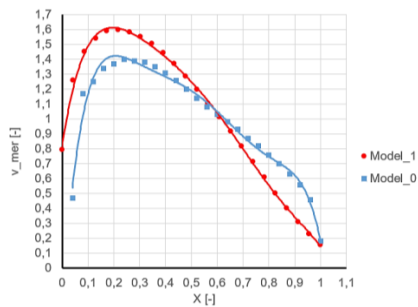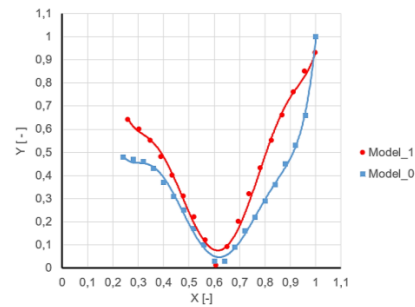
At first sight, the primary difference between the velocity profiles for the both models occur at the location near the second (right) blade where for Model 1 the velocity vectors are more intense than the Model 0, resulting in reduced maximal meridian velocity. Using eq.26, the index of asymmetry is calculated for the observed profiles. Using the individual average velocity, the asymmetry is plotted and compared (fig.36.), where it can be concluded that deviation differences occur between the two observed velocity profiles from their average value, but the velocity profile of Model 0 shows slightly better than the Model 1 (35% vs. 50%) cca. difference of 15% which means that the velocity profile is more symmetric. Theoretically, obtaining more symmetric meridian velocity profile should produce more efficient inflow conditions for the runner. This situation preserves for all other cases and the asymmetry is produced mainly from the shape of the guide vanes. The asymmetry of the profile mostly changes with the guide vanes opening position and flow rate, where for constant guide vane opening and for variable speed conditions, the asymmetry remains almost constant and changes the intensity of the average meridian velocity vector because the changes in the flow rate. This shows that the one dimensional theory of velocity parallelograms is insufficient for describing all the phenomena occurring in the vaneless space.

## 6. Conclusions and Further Work

In this paper, a one-dimensional mathematical model was presented and implemented for development a radial guide vane cascade for the purposes of variable speed high head Francis turbine. For the guide vane hydrofoil geometry, the recommendations for 4 digit NACA hydrofoils were considered and the geometry was obtained by interpolating the camber functions between the guide vanes previously calculated inflow and outflow angles. The obtained geometry is represented as a slightly non-symmetrical concave hydrofoil (Model 1) and it was tested via CFD simulations and compared with the original guide vane hydrofoil (Model 0) from the turbine model Francis 99.

Primarily, the results are interpreted regarding the turbine efficiency, where the developed Model 1 showed better efficiency throughout the operating range of the turbine, for variable speed observed at ±5% change from nominal rotational speed, where at the best efficiency points, the efficiency increased up to 1%. This was obtained because the guide vanes of Model 1 keep higher values of the circulation in front of the runner, which is crucial for high head reaction turbines. Also, Model 1 has minor pressure and energy losses than Model 0 about 1%, which shows that it is hydraulically more efficient. One step further was taken and the meridian velocity profile was examined behind the guide vanes where a 3D deformed velocity field was obtained. By its simplifications, two averaged by height meridian velocity profiles were compared for both models and were statistically examined for deviations of the partial vectors from the average velocity vector, showing the rate of asymmetry in circumferential direction. Model 0 showed 15% more symmetry than Model 1, mainly because the shape of the trailing edge of the guide vanes, and because Model 0 produces lower circulation intensity.

The main conclusions include determination of the crucial parameters which are dominant for developing guide vanes for variable speed high head turbines, such as the intensity of the developed circulation and potentially more symmetrical meridian velocity profile behind the guide vanes for all variable speed operating points, to obtain some kind of law of similarity between the velocity profiles for various rotational speeds, because the laws of velocity parallelograms are insufficient for describing

30th IAHR Symposium on Hydraulic Machinery and Systems

IOP Conf. Series: Earth and Environmental Science **774** (2021) 012112

IOP Publishing

doi:10.1088/1755-1315/774/1/012112

these effects. Further work should include the pressure distribution at the trailing edges of the guide vanes, to prevent occurring of blade tip vortices [12].

The conclusions can be summarized as follows. First, the flow conditions in the vaneless space are far from axisymmetric, but they are repetitive for each guide vane section, which shows that the velocity profiles need to be examined to obtain theoretically close symmetrical meridian velocity profile. Also the average meridian velocity by theory shall be kept constant, which shows that this will influence the flow space between the guide vane blades. After that, the cascade shall be examined if it is accelerating or decelerating the fluid and how does it influence on the efficiency. Second, for high head turbines, the crucial parameter here is shown to be the circulation created by the guide vanes, which need to be increased or decreased for variable speed operations. Finally, the pivot point location and even eccentricity of the guide vanes shall be determined for obtaining "zero torque" on the blade. This condition will change the kinematical point of rotation of the blades, which can lead to reforming the shape of the flow path between two guide vanes, and by that, to change all flow conditions.

## 7. References

[1]  Krivchenko G. I. – Hydraulic Machines - Turbines and Pumps (Mir publishers Moscow, 1986)
[2]  Barlit V. V. – Gidravlichesky turbini (Kiev, 1977)
[3]  Topazh G. I. – Lopastny gydromashini i dydrodynamichesky peredachi – Osnovi rabochego procesa i rascheta gydroturbin (St. Petersburg, Publishing House of the Polytechnic University, 2011)
[4]  Smirnov I. N. – Gydravlichesky turbini i nasosi (Moscow, 1969)
[5]  Lewis R. I. – Vortex element methods for fluid dynamic analysis of engineering systems (Cambridge University Press, 1991)
[6]  BS 1042: Section 2.4. (1989) – Measurement of fluid flow in closed conduits (Part 2. Velocity-area method)
[7]  Stojkovski F., Noshpal A. – Influence of the selected turbulence model on the lift and drag coefficients of parametric developed geometry of 4 digit NACA hydrofoil (19th International Conference On Thermal Science and Engineering of Serbia - Simterm 2019)
[8]  Nordvik A.; Iliev I.; Trivedi C.; Dahlhaug, O. G. (2019) Numerical prediction of hill charts of Francis turbines. Journal of Physics: Conference Series. vol. 1266 (1)
[9]  Iliev I., Trivedi C., Dahlhaug O. G. (2019) Variable-speed operation of Francis turbines: A review of the perspectives and challenges. Renewable & Sustainable Energy Reviews. vol. 103.
[10] Abbot I. H. – National Advisory Committee for Aeronautics - Summary of airfoil data (Report no. 824, 1945)
[11] https://www.ntnu.edu/nvks/francis-99
[12] Rouse H. – Elementary Mechanics of Fluids (Dover Publications Inc. New York, 1946)
[13] IEC 60193 - Hydraulic turbines, storage pumps and pump-turbines – Model acceptance tests
[14] Iliev I., Markov Z. - Grid dependency and relaxation of an iteration procedure for flow calculations in stationary hydraulic turbine parts (Mechanical Engineering Scientific Journal (Skopje); Journal Volume: 32; Journal Issue: 2)